

ULAS J141623.94+134836.3: a Blue T Dwarf Companion to a Blue L Dwarf

Adam J. Burgasser^{1,2}, Dagny Looper^{3,4} and John T. Rayner^{3,4}

ABSTRACT

We confirm the substellar nature of ULAS J141623.94+134836.3, a common proper motion companion to the blue L dwarf SDSS J141624.08+134826.7 identified by Burningham et al. and Scholz. Low-resolution 0.8–2.4 μm spectroscopy obtained with IRTF/SpeX shows strong H₂O and CH₄ absorption bands, consistent with a T7.5 spectral type, and we see possible indications of NH₃ absorption in the 1.0–1.3 μm region. More importantly, the spectrum of ULAS J1416+1348 shows a broadened Y-band peak and highly suppressed K-band flux, both indicative of high surface gravity and/or subsolar metallicity. These traits are verified through spectral model fits, from which we derive atmospheric parameters $T_{\text{eff}} = 650 \pm 60$ K, $\log g = 5.2 \pm 0.4$ cgs, $[\text{M}/\text{H}] \leq -0.3$ and $K_{zz} = 10^4$ cm² s⁻¹, the temperature being significantly warmer than that estimated by Burningham et al. These fits also indicate a model-dependent spectroscopic distance of $10.6^{+3.0}_{-2.8}$ pc for ULAS J1416+1348, formally consistent with the 7.9 ± 1.7 pc astrometric distance for SDSS J1416+1348 from Scholz. The common peculiarities of these two co-spatial, co-moving sources suggest that their unusual blue colors—and those of other blue L and T dwarfs in general—arise from age or metallicity, rather than cloud properties alone.

Subject headings: stars: binaries: visual — stars: fundamental parameters — stars: individual (SDSS J141624.08+134826.7, ULAS J141623.94+134836.3) — stars: low mass, brown dwarfs

¹Center for Astrophysics and Space Science, University of California San Diego, La Jolla, CA 92093, USA; aburgasser@ucsd.edu

²Massachusetts Institute of Technology, Kavli Institute for Astrophysics and Space Research, Building 37, Room 664B, 77 Massachusetts Avenue, Cambridge, MA 02139, USA

³Institute for Astronomy, University of Hawaii, 2680 Woodlawn Drive, Honolulu, HI 96822, USA

⁴Visiting Astronomer at the Infrared Telescope Facility, which is operated by the University of Hawai'i under Cooperative Agreement NCC 5-538 with the National Aeronautics and Space Administration, Office of Space Science, Planetary Astronomy Program

1. Introduction

Over the past 15 years, well over 500 brown dwarf members of the late-M, L and T dwarf spectral classes have been identified in various Galactic environments, encompassing a broad diversity in color, spectral properties, and physical characteristics (Kirkpatrick 2005 and references therein). Sustained effort has been made to identify the coldest of these sources, which include the low-mass extreme of star formation and primordial relics of the Galactic halo population. The most recent discoveries made with the Two Micron All Sky Survey (2MASS; Cutri et al. 2003; Skrutskie et al. 2006), the UKIRT Infrared Deep Sky Survey (UKIDSS; Lawrence et al. 2007) and the Canada France Hawaii Telescope Legacy Survey (CFHTLS; Delorme et al. 2008b) have extended the known population down to and below effective temperatures $T_{eff} \approx 600$ K (e.g., Warren et al. 2007; Burningham et al. 2008, 2009; Burgasser et al. 2008b; Delorme et al. 2008a; Leggett et al. 2009). This has raised the question as to where the currently coldest class of brown dwarfs—the T dwarfs—ends and the next cooler class—the Y dwarfs—might begin. Such exceedingly dim and cold sources are predicted to encompass several major chemical transitions in brown dwarf atmospheres, including the disappearance of Na and K into salt condensates, the emergence of strong NH_3 absorption across the infrared band, and the formation of photospheric water ice clouds (e.g., Marley et al. 1999; Lodders 1999; Lodders & Fegley 2002; Burrows et al. 2003). Accordingly, there is considerable interest and controversy as to how to delineate this putative class; see discussions by Leggett et al. (2007); Burningham et al. (2008) and Delorme et al. (2008a).

A promising low-temperature brown dwarf candidate was recently identified by Burningham et al. (2010) and Scholz (2010) as a co-moving companion to the nearby blue L6 dwarf SDSS J141624.08+134826.7 (hereafter SDSS J1416+1348; Bowler et al. 2010; Schmidt et al. 2010; Kirkpatrick et al. 2010). The object, ULAS J141623.94+134836.3 (hereafter ULAS J1416+1348), was identified in UKIDSS as a faint ($J = 17.35 \pm 0.02$) and unusually blue ($J - K = -1.58 \pm 0.17$) near-infrared source separated by $9''.8$ from the L dwarf. Using astrometry from 2MASS, UKIDSS, the Sloan Digital Sky Survey Data Release 7 (SDSS DR7; York et al. 2000; Abazajian et al. 2009), and follow-up imaging, both Burningham et al. (2010) and Scholz (2010) were able to confirm common proper motion of this pair. Scholz (2010) also determined an astrometric distance to the primary of 7.9 ± 1.7 pc, consistent with spectrophotometric estimates from Bowler et al. (2010, 6.5–10.7 pc) and Schmidt et al. (2010, 6.4–9.6 pc). At this distance, the (poorly constrained) absolute magnitudes of ULAS J1416+1348, $M_J = 17.8 \pm 0.5$ and $M_K = 19.4 \pm 0.5$, are equivalent to or fainter than those of the latest-type brown dwarfs with measured distances, Wolf 940B ($M_J = 17.68 \pm 0.28$ and $M_K = 18.37 \pm 0.28$; Burningham et al. 2009) and ULAS J003402.77–005206.7 ($M_J = 17.65 \pm 0.11$ and $M_K = 17.98 \pm 0.12$; Warren et al. 2007; Smart et al. 2009). Burningham et al. (2010) report a 1.0–2.5 μm spectrum of ULAS J1416+1348, identifying it as a T7.5 brown dwarf with highly

suppressed K -band flux. Indeed, ULAS J1416+1348 is the bluest T dwarf in $J-K$ color identified to date, matching the unusually blue nature of its L dwarf companion. *Spitzer* photometry reported in Burningham et al. (2010) further suggest an exceptionally low-temperature ($T_{eff} \sim 500$ K), metal-poor ($[M/H] \approx -0.3$) and high surface gravity atmosphere ($\log g \approx 5.0-5.3$ cgs).

In this article, we report our measurement of the near-infrared spectrum of ULAS J1416+1348 obtained with the NASA Infrared Telescope Facility (IRTF) SpeX spectrograph (Rayner et al. 2003). This spectrum encompasses the 0.8–2.4 μm region, including the metallicity-sensitive Y -band peak. The unusual shape of this and the K -band flux peak, along with fits to spectral models, affirm the interpretation of this source as a metal-poor, high surface gravity T7.5 brown dwarf, albeit with a T_{eff} that is significantly warmer than that reported by Burningham et al. (2010). In Section 2 we describe our observations and discuss the spectral properties of ULAS J1416+1348, including its classification, spectral anomalies and possible indications of NH_3 absorption in the 1.0–1.3 μm region. In Section 3 we present our spectral model fits to the data and corresponding atmospheric parameters, as well as a model-dependent spectroscopic distance that is in accord with the astrometric distance of the primary. We discuss the relevance of this system with regard to the nature of blue L and T dwarfs in Section 4. Results are summarized in Section 5.

2. Near Infrared Spectroscopy

2.1. Observations and Data Reduction

Low resolution near-infrared spectral data for ULAS J1416+1348 were obtained with SpeX on 2010 January 23 (UT) in mostly clear skies with some light cirrus and $0''.8$ seeing. We used the SpeX prism mode with the $0''.5$ slit aligned to the parallactic angle for all observations, providing 0.7–2.5 μm coverage in a single order with resolution $R \equiv \lambda/\Delta\lambda \approx 120$ and dispersion of 20–30 \AA pixel $^{-1}$. ULAS J1416+1348 was acquired with the slit viewing camera using the J filter and guiding was performed on the nearby primary. A total of 34 exposures of 180 s each were obtained in ABBA dither pairs, nodding along the slit. The first 16 exposures of the source were obtained over an airmass range of 1.28–1.41. We then observed the A0 V star HD 121880 ($V = 7.59$) at an airmass of 1.12 for flux calibration and telluric absorption correction, as well as internal flat field and argon arc lamps for pixel response and wavelength calibration. ULAS J1416+1348 was then reacquired and 18 more exposures made over an airmass range of 1.05–1.13.

Data were reduced with the IDL SpeXtool package, version 3.4 (Cushing et al. 2004),

using standard settings. Due to the faintness of ULAS J1416+1348 and its highly structured spectral morphology, individual spectra were optimally extracted using a trace of HD 121880 as a template. These spectra were then combined using a robust weighted average after scaling each to the median flux at the J -band peak. Telluric absorption and instrumental response corrections were determined from the A0 V spectrum following the method of Vacca et al. (2003), with line-shape kernels derived from the arc lines and adjustments made to the H I line strengths and wavelength scale, as outlined in Cushing et al. (2004).

2.2. The Spectrum of ULAS J1416+1348

The reduced spectrum of ULAS J1416+1348 is shown in Figure 1, compared to equivalent data for the T8 dwarfs 2MASS J04151954–0935066 (hereafter 2MASS J0415–0935; Burgasser et al. 2002, 2004) and 2MASS J09393548–2448279 (hereafter 2MASS J0939–2448; Tinney et al. 2005; Burgasser et al. 2006b). ULAS J1416+1348 exhibits the unambiguous signatures of a T dwarf, with strong H₂O and CH₄ absorption and a blue spectral energy distribution. The 1.6 μ m CH₄ band in the spectrum of ULAS J1416+1348 is slightly weaker than those of the T8 comparison sources, although the breadth of the J - and H -band peaks (both shaped by the wings of H₂O and CH₄ bands) are equivalent to the spectrum of 2MASS J0415–0935. T dwarf classification indices (Burgasser et al. 2006b) indicate a spectral type of T7.5 \pm 0.5 for this source, which is also consistent with its NH₃-H and W_J indices (Table 1; Warren et al. 2007; Burningham et al. 2008; Delorme et al. 2008a). This classification and most of the spectral indices are in agreement with those determined by Burningham et al. (2010). However, we find a significant disagreement in our measurement of the CH₄-J index. Burningham et al. (2010) specifically note this index as anomalous whereas our value is consistent with the overall spectral classification of ULAS J1416+1348. As both spectra were obtained at roughly the same resolution ($\lambda/\Delta\lambda \approx 100$), and signal-to-noise of the SpeX data in the Y -, J - and H -band peaks is good (~ 40 – 70), the origin of this anomaly is unclear.

What is most remarkable about the spectrum of ULAS J1416+1348 is the breadth of its 1.07 μ m Y -band flux peak and strongly suppressed 2.10 μ m K -band flux peak. The latter feature was also noted in the spectral data of Burningham et al. (2010), and explains the very blue $J - K$ color of the source; we calculate a spectrophotometric color of $J - K = -1.71 \pm 0.23$ ¹ from our SpeX spectrum, consistent with both the UKIDSS photom-

¹This value was determined by calculating the colors of 100 realizations of the spectral data, with fluxes varied following a normal distribution of the noise spectrum. We report here the mean and standard deviation

etry and measurements by Burningham et al. (2010). The broadened *Y*-band peak in the spectrum of ULAS J1416+1348 is readily apparent, and similar to but more extreme than the broadened peak seen in the spectrum of 2MASS J0939–2448 (Figure 1; see also Figure 2 in Burgasser et al. 2006a). The origins of both features are discussed below.

2.3. NH₃ Absorption in the 1.0–1.3 μm Region?

In addition to these broad spectral anomalies, we identified several intriguing absorption features around the *Y*-, *J*- and *H*-band flux peaks in the spectrum of ULAS J1416+1348. As shown in Figure 2, these features are at 0.997, 1.039, 1.072, 1.232, 1.249, 1.292, 1.302 and 1.570 μm, none of which are present in the late-type T dwarfs with comparable SpeX data.² Among these features, the 1.072, 1.232 and 1.570 μm features are also seen in the absorption spectrum of Jupiter (Rayner et al. 2009). Given tentative suggestions of the onset of NH₃ absorption in the near-infrared spectra of the latest-type T dwarfs (Saumon et al. 2000; Leggett et al. 2007; Delorme et al. 2008a), we examined whether any of these features might be coincident with NH₃ opacity. Figure 2 overlays the laboratory transmission function of NH₃ from Irwin et al. (1999), measured at temperatures of 200–300 K and pressures of 0.01–1 bar. Structure in the NH₃ spectrum appears to be coincident with some of the features, most notably the 0.997, 1.039 and prominent 1.072 μm dips in the *Y*-band, and the weaker 1.292 and 1.302 μm dips in the *J*-band. However, strong NH₃ opacity features, such as the 1.01–1.05 and 1.19–1.23 μm bands, are not seen in the data.

There are important caveats to such comparisons of opacity measurements to low-resolution brown dwarf spectra. First, opacity from several species, most notably H₂O and CH₄ gas, blankets the entire near-infrared region, and the resolution of the SpeX data makes it impossible to separate narrow features from these species from coincident absorption arising from NH₃. Second, the laboratory measurements of Irwin et al. (1999) were obtained in very different gas conditions than those that characterize the warmer photospheres of T dwarfs, and are not likely to include the higher angular momentum states expected in to be present in brown dwarf spectra. Indeed, Leggett et al. (2007) have shown that current brown dwarf models incorporating the Irwin et al. (1999) opacities predict NH₃ bands that are much stronger than observed, even when nonequilibrium abundances due to vertical mixing are considered (Saumon et al. 2006; Hubeny & Burrows 2007).

of these measures.

²See <http://www.browndwarfs.org/spexprism>.

In summary, while these features are notable, they cannot be conclusively associated with NH_3 absorption. Higher resolution spectra coupled with better opacity data are needed to verify their origin.

3. The Physical Properties of ULAS J1416+1348

3.1. Qualitative indicators of High Surface Gravity and Subsolar Metallicity

The broadened Y -band and suppressed K -band peaks in the spectrum of ULAS J1416+1348 are similar in nature to those seen in previously identified, unusually blue T dwarfs, and are indicative of pressure effects related to surface gravity and metallicity (Burgasser et al. 2002, 2006a; Knapp et al. 2004; Chiu et al. 2006; Leggett et al. 2007; Stephens et al. 2009). K -band flux is regulated by collision-induced H_2 absorption (Linsky 1969; Saumon et al. 1994; Borysow 2002), which is sensitive to both photospheric gas temperature and pressure. The short wavelength slope of the Y -band peak is shaped by the red wing of the pressure-broadened $0.77 \mu\text{m}$ K I doublet, which is also modulated by temperature (affecting the K abundance) and pressure (affecting the pressure-broadened wings; Allard et al. 2003; Burrows & Volobuyev 2003). The Y -band peak has been specifically noted as being metallicity-sensitive in comparison of synthetic atmosphere models, becoming both broadened and blue-shifted for lower metallicities (Burgasser et al. 2006a; Leggett et al. 2007).

The archetype blue T dwarf, 2MASS J09373487+2931409 (hereafter 2MASS J0937+2931; Burgasser et al. 2002) exhibits the same Y -band and K -band anomalies as ULAS J1416+1348 and, importantly, is consistently well-matched to models with subsolar metallicities ($[\text{M}/\text{H}] = -0.1$ to -0.4) and high surface gravities ($\log g = 5.2$ to 5.5 ; Burgasser et al. 2006a; Geballe et al. 2009). 2MASS J0939–2448 also exhibits these peculiarities (Figure 1), and its near- and mid-infrared spectrum is well-matched to subsolar metallicity models as well, although it is additionally suspected of being an unresolved binary (Burgasser et al. 2008b; Leggett et al. 2009). Importantly, the Y -band and K -band anomalies are more pronounced in the spectrum of ULAS J1416+1348 than in those of 2MASS J0937+2931 and 2MASS J0939–2448. Our measure of the K/J index—the relative flux between the J - and K -band peaks—is the smallest reported to date: 0.037 ± 0.004 compared to 0.059 for 2MASS J0939–2448 (see Table 6 in Burgasser et al. 2006b and Table 6 in Burningham et al. 2009). These measures suggest that ULAS J1416+1348 is a true outlier in terms of its physical properties.

3.2. Comparison to Spectral Models

To quantify these properties, we compared the spectrum of ULAS J1416+1348 to the atmosphere models of Saumon & Marley (2008). We followed the prescriptions detailed in Cushing et al. (2008) and Burgasser et al. (2008b), comparing our SpeX spectrum, flux-calibrated to the *J*-band photometry reported in Burningham et al. (2010), to models spanning temperatures $T_{eff} = 500\text{--}1000$ K (50 K steps); surface gravities $\log g = 4.0\text{--}5.5$ cgs (0.5 dex steps); metallicities $[M/H] = -0.3, 0$ and $+0.3$ dex relative to Solar; and vertical diffusion coefficients $K_{zz} = 0$ and 10^4 cm² s⁻¹ (see Saumon et al. 2006). The models were smoothed to the resolution of the SpeX data using a Gaussian kernel, and interpolated onto a common wavelength scale. Fits were made exclusively to the 0.9–2.4 μm region. The goodness-of-fit statistic G_k (Cushing et al. 2008) was used to gauge the agreement between models and data, and we followed the same weighting scheme employed by those authors in which each pixel is weighted by its breadth in wavelength space. Model surface fluxes were scaled by the factor $C_k = (R/d)^2$ which minimizes G_k (Equation 2 in Cushing et al. 2008), where R is the radius of the brown dwarf and d its distance from the Earth. Fits were made to all 264 models. Distributions of the fit parameters were generated following a weighting scheme similar to that described in Burgasser et al. (2008b), in which each model’s parameters were incorporated into the distributions with a weight proportional to $3 e^{-0.5G_k}$. To examine the robustness of our fits to observational uncertainties, we also performed a Monte Carlo simulation similar to that described in Cushing et al. (2008) and Bowler et al. (2009), generating 1000 realizations of the spectrum with fluxes randomly varied about the measured values following a normal distribution of the observational noise; the overall scaling of the spectrum was also varied following a normal distribution tied to the uncertainty in the *J*-band photometry. These spectra were compared to the 20 models that best fit the original spectrum, and distributions of the resulting best-fit parameter sets and C_k scale factors were determined.

Table 2 summarizes the parameters of the ten best-fitting spectral models, while Figure 3 shows the overall best-fit model overlaid on the spectrum of ULAS J1416+1348: $T_{eff} = 650$ K, $\log g = 5.0$ cgs, $[M/H] = -0.3$ and $K_{zz} = 10^4$ cm² s⁻¹. This model was the best fit for all of the spectra in our Monte Carlo simulation; i.e., its Monte Carlo fraction $f_{MC} = 1.000$ (Cushing et al. 2008). It is a reasonably good match to the spectral energy distribution, qualitatively reproducing the strong absorption bands, broadened *Y*-band peak and suppressed *K*-band peak, although the *H*-band peak flux is $\sim 10\text{--}15\%$ underestimated.

³Note that in Burgasser et al. (2008b), the weighting function was $e^{-0.1G_k}$, a conservative choice that favored poorer-fitting models more highly. The 0.5 coefficient used here is more consistent with the probability distribution function of the χ^2 statistic, for which G_k is a close analog.

The parameter distributions from all of the model fits are also shown in Figure 3. Gaussian fits to these distributions yield optimal parameters of $T_{eff} = 650 \pm 60$ K and $\log g = 5.2 \pm 0.4$ cgs. The metallicity distribution clearly favors a metal-poor atmosphere; the five best-fitting models all have a subsolar metallicity. In fact, the one-sided distribution in our limited model set means that we cannot rule out metallicities less than -0.3 . The model fits also indicate some vertical mixing is present, favoring $K_{zz} = 10^4 \text{ cm}^2 \text{ s}^{-1}$ over $0 \text{ cm}^2 \text{ s}^{-1}$, although a strict constraint cannot be made.

With respect to surface gravity and metallicity, our fits to the spectrum of ULAS J1416+1348 are in agreement with the estimates of Burningham et al. (2010), indicating that this unusually blue T dwarf is likely to be old, massive and metal-poor. The derived T_{eff} and $\log g$ parameters and their uncertainties correspond to an age of 2–10 Gyr and a mass of 0.021–0.045 M_{\odot} according to the evolutionary models of Baraffe et al. (2003). This age is consistent with membership in the Galactic disk population, as previously suggested by the system’s kinematics (Bowler et al. 2010; Schmidt et al. 2010). The subsolar metallicity favored by the model fits is in quantitative agreement with spectral analyses of other blue T dwarfs, as well as characterization of the L dwarf companion, SDSS J1416+1348, which does not appear to be a full-fledged L subdwarf (Bowler et al. 2010; however, see Kirkpatrick et al. 2010). As such, these fits support our qualitative analysis of the spectrum: the spectral peculiarities and blue color of ULAS J1416+1348 appear to be the result of a high pressure atmosphere arising from high surface gravity and subsolar metallicity.

3.3. The T_{eff} of ULAS J1416+1348

Our inferred T_{eff} for ULAS J1416+1348 is somewhat low for T7–T8 dwarfs, which typically have $T_{eff} \approx 700\text{--}900$ K (Golimowski et al. 2004; Vrba et al. 2004; Stephens et al. 2009). This is likely to be a surface gravity and/or metallicity effect. Burgasser et al. (2006a) have previously found that late-type T dwarfs with higher surface gravities tend to have lower T_{eff} s for a given spectral type. Burningham et al. (2010), on the other hand, derive an even lower temperature for ULAS J1416+1348, $T_{eff} \approx 500$ K, based on this source’s uniquely red $H\text{--}[4.5]$ color. The link between T_{eff} and $H\text{--}[4.5]$ color for brown dwarfs cooler than ~ 1000 K was originally established by Warren et al. (2007), and has been shown to provide increased sensitivity for the latest-type T dwarfs (Stephens et al. 2009; Leggett et al. 2010). However, Leggett et al. (2009) have noted that metallicity effects are relevant and can shift $H\text{--}[4.5]$ to the red by roughly 0.1 mag for every 0.1 dex decrement in metallicity (see also Figure 6 in Burningham et al. 2010). If ULAS J1416+1348 has a metallicity significantly below $[M/H] = -0.3$ —not ruled out by the present model fits—then this characteristic may

have as much to do with its extreme color as its low temperature. It is relevant to note that the [3.6]-[4.5] color of ULAS J1416+1348, another T_{eff} indicator (Patten et al. 2006), is not an extremum; this source is in fact bluer than 2MASS J0939–2448. This may be an indication that the 3.3 μm CH_4 band, like the 1.6 μm band, is relatively weak compared to other T8-T9 dwarfs, consistent with a warmer T_{eff} . However, metallicity and/or surface gravity effects may again complicate a strict correlation.

The Saumon & Marley (2008) spectral model based on the atmosphere parameters favored by Burningham et al. (2010)— $T_{eff} = 500$ K, $\log g = 5.0$ cgs, $[\text{M}/\text{H}] = -0.3$ dex and $K_{zz} = 10^4 \text{ cm}^2 \text{ s}^{-1}$ —is also shown in Figure 3. The cooler model actually provides a better match to the relative flux between the J - and H -band peaks and the width of the J -band peak; but predicts stronger 1.6 μm CH_4 absorption, a far more distorted Y -band peak and a more suppressed K -band flux peak than observed. These deviations make this model a 2σ outlier compared to the best-fit model for our data. We emphasize that the differences between these fits do not explicitly rule out either set of parameters. It is well known that incomplete opacity tables, inaccurate treatment of K I pressure broadening and the influence of distributed condensate opacity (“cloud tops”) can result in poor fits to T dwarf near-infrared spectra (Burgasser et al. 2006a; Saumon et al. 2007; Cushing et al. 2008; Stephens et al. 2009). However, to the limits of the accuracy of the current spectral models, our analysis favors a warmer temperature for ULAS J1416+1348 than indicated by its H -[4.5] color.

3.4. Spectroscopic Distance

Following Bowler et al. (2009), we calculated a spectroscopic parallax for ULAS J1416+1348 using the model-to-data flux scaling factor C_k derived from the spectral modeling. The mean value and uncertainty of this factor (based on the same G_k weighting scheme used for the parameter distributions) yields a distance-to-radius ratio $d/R = 12.8 \pm 3.0 \text{ pc}/R_{Jup}$. Based on the inferred T_{eff} and $\log g$ range, the evolutionary models of Saumon & Marley (2008) predict a radius $R = 0.83^{+0.14}_{-0.10} R_{Jup}$, corresponding to a distance of $10.6^{+3.0}_{-2.8} \text{ pc}$. This is larger than but within 1σ of the astrometric distance of the primary from Scholz (2010), $7.9 \pm 1.7 \text{ pc}$. In contrast, the 500 K model shown in Figure 3 requires $d/R = 5.8 \text{ pc}/R_{Jup}$, and the corresponding $R = 0.73 R_{Jup}$ implies a distance of only 4.2 pc, significantly smaller than both spectrophotometric and astrometric estimates for SDSS J1416+1348. Hence, to the limits of the accuracy of the spectral and evolutionary models of Saumon & Marley (2008), our atmospheric parameter determinations for ULAS J1416+1348 are commensurate with this source being cospatial with its co-moving L dwarf companion.

4. The Nature of Blue L and T Dwarfs

The SDSS J1416+1348/ULAS J1416+1348 system provides a unique opportunity to explore the underlying physical properties that distinguish blue L and T dwarfs. While surface gravity and metallicity effects have long been acknowledged as contributors to the peculiarities of blue T dwarfs, condensate cloud properties have been seen as playing a more important role in shaping the spectra of blue L dwarfs. Several studies have argued that thin and/or patchy condensate clouds in the photospheres of blue L dwarfs adequately explain their unique photometric and spectroscopic characteristics (Knapp et al. 2004; Cruz et al. 2007; Burgasser et al. 2008a; Stephens et al. 2009). However, thin clouds cannot be responsible for the colors and spectra of late-type blue T dwarfs—such as ULAS J1416+1348—since clouds are buried deep below the visible photosphere in these low-temperature objects (Ackerman & Marley 2001).

The distinct empirical characteristics shared by SDSS J1416+1348 and ULAS J1416+1348 must have an origin that is common to both sources; this argues for age and/or metallicity. Older ages for blue L and T dwarfs are supported by their collective kinematics; Faherty et al. (2009) and Kirkpatrick et al. (2010) have shown that this subgroup exhibits a much broader range of tangential velocities ($\sigma_V \approx 50 \text{ km s}^{-1}$) than L and T dwarfs with “normal” colors ($\sigma_V \approx 22 \text{ km s}^{-1}$). The high surface gravities inferred from spectral model fits to blue L and T dwarfs further support older ages for these sources (e.g., Burgasser et al. 2008b; Cushing et al. 2008; Geballe et al. 2009). Subsolar metallicities are also supported by spectral model fits to blue T dwarfs, and the fact that blue L dwarfs exhibit spectral characteristics that are intermediate between normal field L dwarfs and halo L subdwarfs (Burgasser 2004; Kirkpatrick et al. 2010). However, the discovery of a blue L5 dwarf companion to the solar-metallicity field M4.5 star G 203-50 (Radigan et al. 2008) suggests that metallicity does not play a consistent role in shaping these spectra.

We argue that the common photometric and spectroscopic properties of SDSS J1416+1348 and ULAS J1416+1348 favors old age, and possibly subsolar metallicity, as the physical trait that characterizes the blue L and T dwarf populations. Thin condensate clouds may still be common for blue L dwarf atmospheres, with higher surface gravities and subsolar metallicities contributing to increased sedimentation rates and a reduced supply of condensate species, respectively. However, our conjecture predicts that these cloud properties are simply a consequence of the high-pressure photospheres characterizing old, high surface gravity and—in some cases—metal-poor brown dwarfs.

5. Summary

We have measured the 0.8–2.4 μm spectrum of ULAS J1416+1348, the common proper motion companion to the blue L dwarf SDSS J1416+1348. These data confirm the T7.5 spectral type determined by Burningham et al. (2010), show possible NH_3 features in the 1.0–1.3 μm region, and reveal broadened Y -band and highly suppressed K -band peaks consistent with a high surface gravity and/or subsolar metallicity. Spectral model fits based on calculations by Saumon & Marley (2008) indicate atmospheric parameters $T_{\text{eff}} = 650 \pm 60$ K, $\log g = 5.2 \pm 0.4$ cgs, $[\text{M}/\text{H}] \leq -0.3$ and $K_{zz} = 10^4 \text{ cm}^2 \text{ s}^{-1}$. The metallicity and surface gravity are consistent with the analysis by Burningham et al. (2010), but our T_{eff} is ~ 150 K (2.5σ) warmer. If correct, it suggests that the extreme H -[4.5] color of this source may be due to metallicity and/or surface gravity effects, rather than an exceedingly low T_{eff} . Our fit parameters for ULAS J1416+1348 imply a model-dependent spectroscopic distance that is formally consistent with the astrometric distance of SDSS J1416+1348 measured by Scholz (2010), and further strengthens the case that this pair is a coeval system of unusually blue brown dwarfs. We argue that the common peculiarities of the SDSS J1416+1348/ULAS J1416+1348 system implies that most unusually blue L and T dwarfs derive their unique properties from old age, and possibly subsolar metallicity, with the thin clouds of blue L dwarfs being a secondary effect.

Despite the substantial amount of follow-up already done for this fairly recent discovery, its benchmark role in understanding temperature, surface gravity, metallicity and cloud effects in L and T dwarf spectra motivates further observational study of both components. These include independent parallax measurements to verify absolute fluxes; higher-resolution near-infrared spectroscopy and mid-infrared spectroscopy of the secondary to validate potential NH_3 features and discern the origin of its unusual mid-infrared colors; broad-band spectral energy distribution measurements of both components to measure luminosities and constrain T_{eff} s; high-resolution imaging to search for additional components; and improved model fits to better constrain atmospheric parameters. In addition, the ~ 100 AU projected separation of this system—wider than any L dwarf/T dwarf pair identified to date—raises questions as to the formation of it and other widely-separated, very low-mass stellar/brown dwarf multiples (e.g., Luhman 2004; Billères et al. 2005; Close et al. 2007). Coupled with its proximity to the Sun, the SDSS J1416+1348/ULAS J1416+1348 system is a target of opportunity for studies of cold brown dwarf atmospheres and origins.

The authors acknowledge telescope operator Dave Griep at IRTF for his assistance with the observations; B. Burningham for providing an electronic version of the Irwin et al. NH_3 opacity spectrum, and D. Saumon for providing electronic copies of the spectral and

evolutionary models used in the analysis. This research has benefitted from the M, L, and T dwarf compendium housed at DwarfArchives.org and maintained by Chris Gelino, Davy Kirkpatrick, and Adam Burgasser; the SpeX Prism Spectral Libraries, maintained by Adam Burgasser at <http://www.browndwarfs.org/spexprism>; and the VLM Binaries Archive maintained by Nick Siegler at <http://www.vlmbinaries.org>. The authors recognize and acknowledge the very significant cultural role and reverence that the summit of Mauna Kea has always had within the indigenous Hawaiian community. We are most fortunate to have the opportunity to conduct observations from this mountain.

Facilities: IRTF (SpeX)

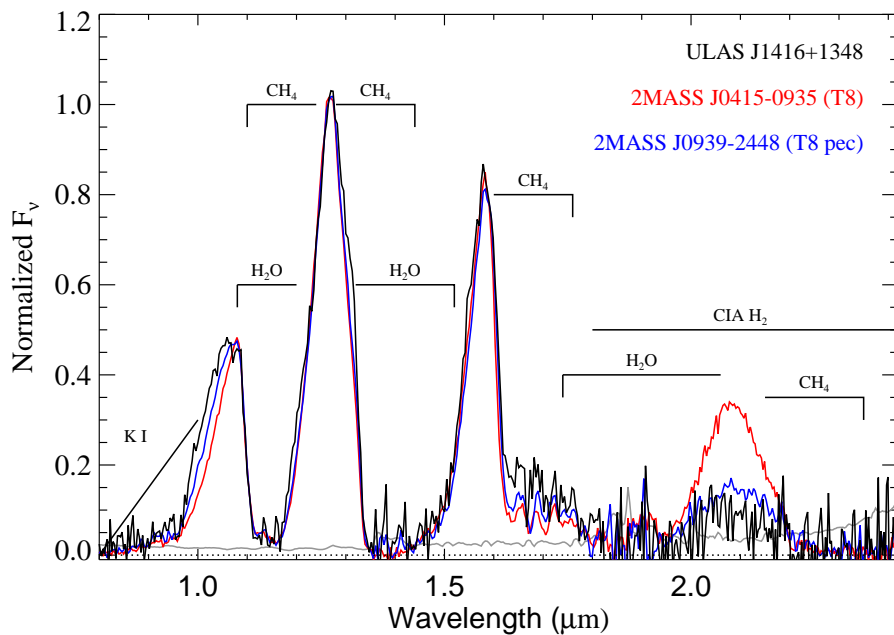


Fig. 1.— SpeX prism spectrum of ULAS J1416+1348 (black line) compared to equivalent data for the T8 dwarfs 2MASS J0415–0935 (red line; Burgasser et al. 2004) and 2MASS J0939–2448 (blue line; Burgasser et al. 2006b). All three spectra are normalized at $1.27 \mu\text{m}$, and the corresponding noise spectrum for ULAS J1416+1348 is indicated by the light grey line. Prominent H₂O and CH₄ absorption features are labeled, as well as the region influenced by the pressure-broadened K I doublet wing ($\lambda \lesssim 1 \mu\text{m}$) and collision-induced H₂ opacity ($\lambda \gtrsim 1.75 \mu\text{m}$).

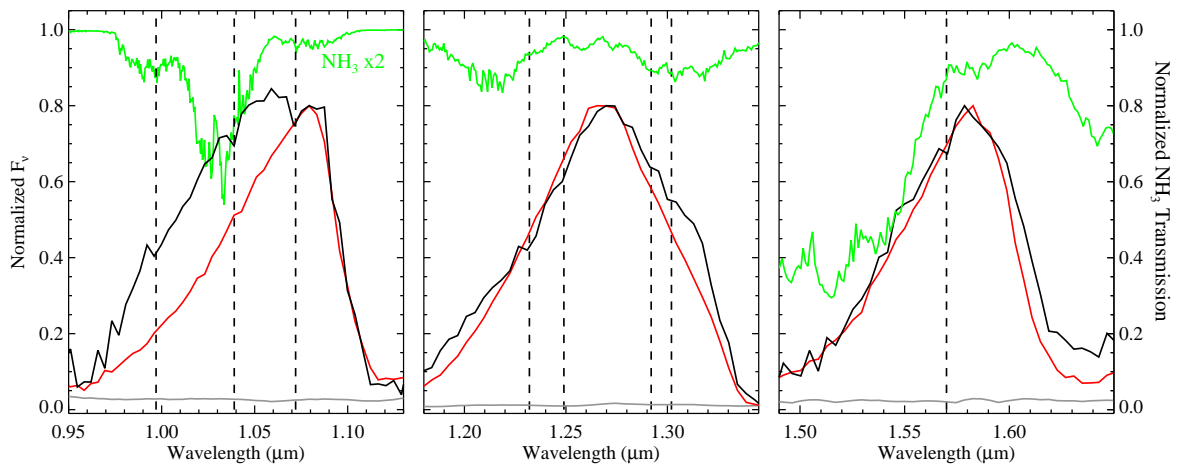


Fig. 2.— Close-up views of the $1.07 \mu\text{m}$ (*Y*-band, left), $1.27 \mu\text{m}$ (*J*-band, middle) and $1.58 \mu\text{m}$ (*H*-band, right) flux peaks in the spectra of ULAS J1416+1348 (black line) and 2MASS J0415–0935 (red line). Data are normalized in each panel to the peak flux in the given band. Also shown is the normalized transmission spectrum of NH_3 from Irwin et al. (1999). The transmission is magnified by a factor of two in the *Y*-band panel to highlight weaker bands. The absorption features in the spectrum of ULAS J1416+1348 noted in the text are indicated by dashed lines.

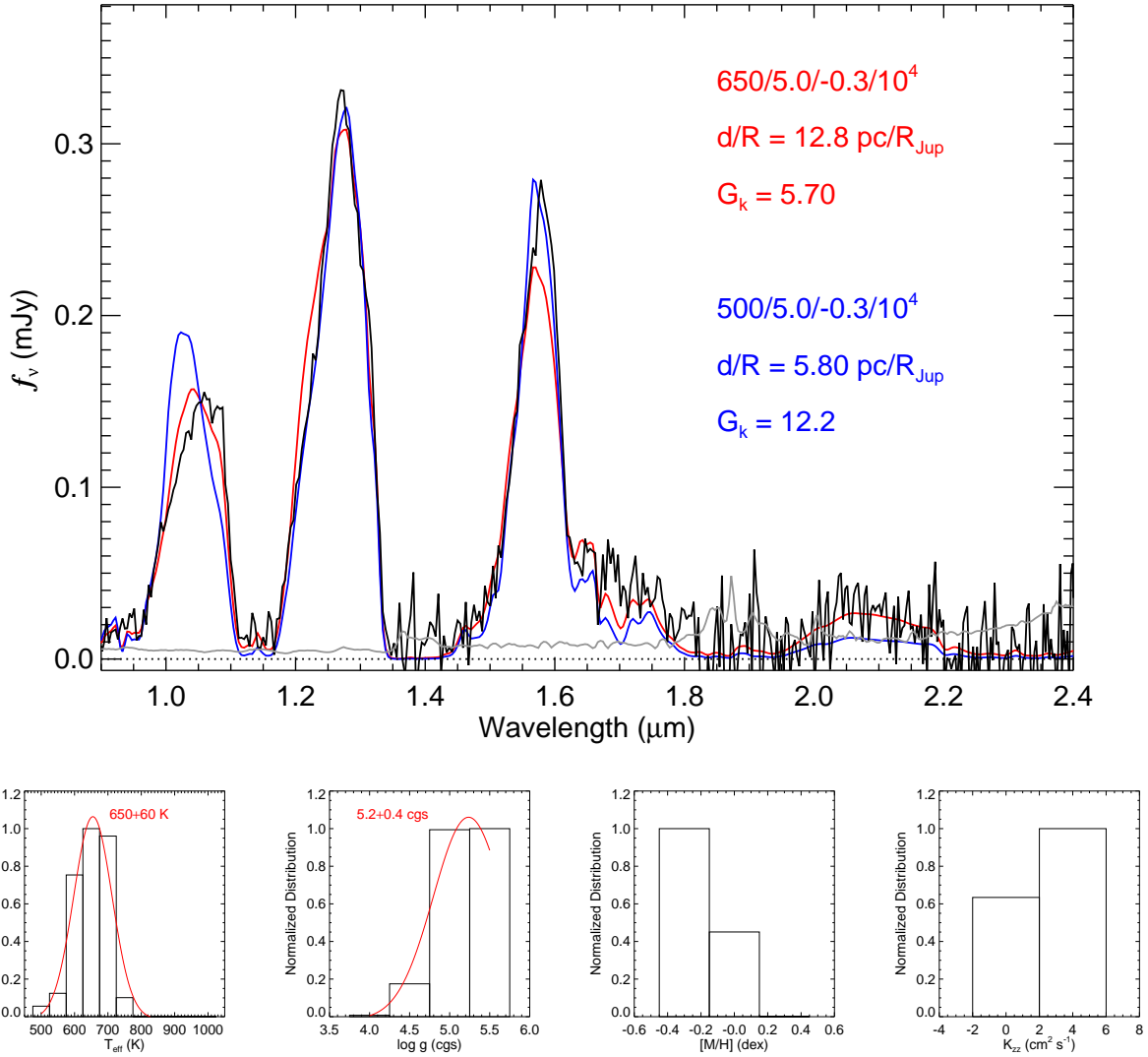


Fig. 3.— (Top panel): Best-fitting model spectrum (red line) to our SpeX spectrum of ULAS J1416+1348 (black line): $T_{\text{eff}} = 650 \text{ K}$, $\log g = 5.0 \text{ cgs}$, $[M/H] = -0.3$ and $K_{zz} = 10^4 \text{ cm}^2 \text{ s}^{-1}$; and the model corresponding to the parameters of Burningham et al. (2010): $T_{\text{eff}} = 500 \text{ K}$, $\log g = 5.0 \text{ cgs}$, $[M/H] = -0.3$ and $K_{zz} = 10^4 \text{ cm}^2 \text{ s}^{-1}$. The data are scaled to J -band photometry from Burningham et al. (2010) and the models are scaled to minimize G_k values (indicated). The noise spectrum for ULAS J1416+1348 is indicated by the grey line. (Bottom panels): Parameter distributions of (left to right) T_{eff} , $\log g$, $[M/H]$ and K_{zz} based on the weighting scheme described Burgasser et al. (2008b) and in the text. Means and uncertainties for T_{eff} and $\log g$ are indicated in the first two panels and are based on Gaussian fits to the distributions. The metallicity distribution is such that we can only conclude that $[M/H] \leq -0.3$, while the K_{zz} distribution indicates a slight preference for $K_{zz} = 10^4 \text{ cm}^2 \text{ s}^{-1}$.

Table 1. Spectral Indices for ULAS J1416+1348.

Index	Value ^a	SpT	Value B10 ^b	Reference
H ₂ O-J	0.053±0.008	T8	0.07±0.01	1
CH ₄ -J	0.268±0.006	T7	0.34±0.01	1
W_J	0.376±0.005	T7	0.34±0.01	2,3
H ₂ O-H	0.181±0.011	T8	0.20±0.01	1
CH ₄ -H	0.197±0.010	T7	0.20±0.01	1
NH ₃ -H	0.675±0.014	...	0.61±0.01	4
CH ₄ -K	0.085±0.144	T7	0.29±0.02	1
K/J	0.037±0.004	1

^aSpectral index values were measured for 1000 realizations of the spectrum, each with a normal distribution of random values scaled by the noise spectrum added to the original fluxes. The reported values are the means and standard deviations of these measurements.

^bSpectral index values reported in Burningham et al. (2010) based on $\lambda/\Delta\lambda \approx 100$ near-infrared spectral data.

References. — (1) Burgasser et al. (2006b); (2) Warren et al. (2007); (3) Burningham et al. (2008); (4) Delorme et al. (2008b).

Table 2. Ten Best-Fitting Saumon & Marley (2008) Spectral Models to SpeX Data for ULAS J1416+1348.

Rank	T_{eff} (K)	$\log g$ (cgs)	[M/H] (dex)	K_{zz} ($\text{cm}^2 \text{s}^{-1}$)	G_k	d/R (pc/ R_{Jup})
1 ^a	650	5.0	-0.3	10^4	5.70	12.8
2	700	5.0	-0.3	10^4	5.97	15.5
3	600	5.0	-0.3	10^4	6.10	10.2
4	700	5.0	-0.3	0	6.53	15.4
5	650	5.0	-0.3	0	6.58	12.7
6	600	5.5	0.0	10^4	6.85	10.5
7	650	5.5	0.0	10^4	6.88	13.3
8	700	5.5	0.0	10^4	7.31	15.7
9	600	5.0	-0.3	0	7.37	10.2
10	650	5.5	0.0	0	8.01	13.3
Avg. ^b	650 ± 60	5.2 ± 0.4	≤ -0.3	$\sim 10^4$...	12.8 ± 3.0

^aBest-fitting model for 1000 synthesized spectra in Monte Carlo simulation; i.e., $f_{MC} = 1.000$ (see Cushing et al. 2008).

^bBased on the weighted parameter distributions shown in Figure 3. Each model contributes its parameters to the distributions scaled by the factor $e^{-0.5G_k}$. The means and uncertainties of T_{eff} and $\log g$ were determined by Gaussian fits to their respective distributions (see Burgasser et al. 2008b). The [M/H] distribution peaked at the lower limit of the sampled parameter space, while the models slightly favor $K_{zz} = 10^4 \text{ cm}^2 \text{ s}^{-1}$ over $0 \text{ cm}^2 \text{ s}^{-1}$.

REFERENCES

- Abazajian, K. N., et al. 2009, *ApJS*, 182, 543
- Ackerman, A. S., & Marley, M. S. 2001, *ApJ*, 556, 872
- Allard, N. F., Allard, F., Hauschildt, P. H., Kielkopf, J. F., & Machin, L. 2003, *A&A*, 411, L473
- Baraffe, I., Chabrier, G., Barman, T. S., Allard, F., & Hauschildt, P. H. 2003, *A&A*, 402, 701
- Billères, M., Delfosse, X., Beuzit, J.-L., Forveille, T., Marchal, L., & Martín, E. L. 2005, *A&A*, 440, L55
- Borysow, A. 2002, *A&A*, 390, 779
- Bowler, B. P., Liu, M. C., & Cushing, M. C. 2009, *ApJ*, 706, 1114
- Bowler, B. P., Liu, M. C., & Dupuy, T. J. 2010, *ApJ*, 710, 45
- Burgasser, A. J. 2004, *ApJ*, 614, L73
- Burgasser, A. J., Burrows, A., & Kirkpatrick, J. D. 2006a, *ApJ*, 639, 1095
- Burgasser, A. J., Geballe, T. R., Leggett, S. K., Kirkpatrick, J. D., & Golimowski, D. A. 2006b, *ApJ*, 637, 1067
- Burgasser, A. J.,Looper, D. L., Kirkpatrick, J. D., Cruz, K. L., & Swift, B. J. 2008a, *ApJ*, 674, 451
- Burgasser, A. J., McElwain, M. W., Kirkpatrick, J. D., Cruz, K. L., Tinney, C. G., & Reid, I. N. 2004, *AJ*, 127, 2856
- Burgasser, A. J., Tinney, C. G., Cushing, M. C., Saumon, D., Marley, M. S., Bennett, C. S., & Kirkpatrick, J. D. 2008b, *ApJ*, 689, L53
- Burgasser, A. J., et al. 2002, *ApJ*, 564, 421
- Burningham, B., et al. 2008, *MNRAS*, 391, 320
- . 2009, *MNRAS*, 395, 1237
- . 2010, ArXiv e-prints

- Burrows, A., Sudarsky, D., & Lunine, J. I. 2003, *ApJ*, 596, 587
- Burrows, A., & Volobuyev, M. 2003, *ApJ*, 583, 985
- Chiu, K., Fan, X., Leggett, S. K., Golimowski, D. A., Zheng, W., Geballe, T. R., Schneider, D. P., & Brinkmann, J. 2006, *AJ*, 131, 2722
- Close, L. M., et al. 2007, *ApJ*, 660, 1492
- Cruz, K. L., et al. 2007, *AJ*, 133, 439
- Cushing, M. C., Marley, M. S., Saumon, D., Kelly, B. C., Vacca, W. D., Rayner, J. T., Freedman, R. S., Lodders, K., & Roellig, T. L. 2008, *ApJ*, 678, 1372
- Cushing, M. C., Vacca, W. D., & Rayner, J. T. 2004, *PASP*, 116, 362
- Cutri, R. M., et al. 2003, *VizieR Online Data Catalog*, 2246, 0
- Delorme, P., et al. 2008a, *A&A*, 482, 961
- . 2008b, *A&A*, 484, 469
- Faherty, J. K., Burgasser, A. J., Cruz, K. L., Shara, M. M., Walter, F. M., & Gelino, C. R. 2009, *AJ*, 137, 1
- Geballe, T. R., Saumon, D., Golimowski, D. A., Leggett, S. K., Marley, M. S., & Noll, K. S. 2009, *ApJ*, 695, 844
- Golimowski, D. A., et al. 2004, *AJ*, 127, 3516
- Hubeny, I., & Burrows, A. 2007, *ApJ*, 669, 1248
- Irwin, P. G. J., Calcutt, S. B., Sihra, K., Taylor, F. W., Weir, A. L., Ballard, J., & Johnston, W. B. 1999, *Journal of Quantitative Spectroscopy and Radiative Transfer*, 62, 193
- Kirkpatrick, J. D. 2005, *ARA&A*, 43, 195
- Kirkpatrick, J. D., et al. 2010, *ApJ*, submitted
- Knapp, G. R., et al. 2004, *AJ*, 127, 3553
- Lawrence, A., et al. 2007, *MNRAS*, 379, 1599
- Leggett, S. K., Marley, M. S., Freedman, R., Saumon, D., Liu, M. C., Geballe, T. R., Golimowski, D. A., & Stephens, D. C. 2007, *ApJ*, 667, 537

- Leggett, S. K., et al. 2009, *ApJ*, 695, 1517
- . 2010, ArXiv e-prints
- Linsky, J. L. 1969, *ApJ*, 156, 989
- Lodders, K. 1999, *ApJ*, 519, 793
- Lodders, K., & Fegley, B. 2002, *Icarus*, 155, 393
- Luhman, K. L. 2004, *ApJ*, 614, 398
- Marley, M. S., Gelino, C., Stephens, D., Lunine, J. I., & Freedman, R. 1999, *ApJ*, 513, 879
- Patten, B. M., et al. 2006, *ApJ*, 651, 502
- Radigan, J., Lafrenière, D., Jayawardhana, R., & Doyon, R. 2008, *ApJ*, 689, 471
- Rayner, J. T., Cushing, M. C., & Vacca, W. D. 2009, *ApJS*, 185, 289
- Rayner, J. T., Toomey, D. W., Onaka, P. M., Denault, A. J., Stahlberger, W. E., Vacca, W. D., Cushing, M. C., & Wang, S. 2003, *PASP*, 115, 362
- Saumon, D., Bergeron, P., Lunine, J. I., Hubbard, W. B., & Burrows, A. 1994, *ApJ*, 424, 333
- Saumon, D., Geballe, T. R., Leggett, S. K., Marley, M. S., Freedman, R. S., Lodders, K., Fegley, Jr., B., & Sengupta, S. K. 2000, *ApJ*, 541, 374
- Saumon, D., & Marley, M. S. 2008, *ApJ*, 689, 1327
- Saumon, D., Marley, M. S., Cushing, M. C., Leggett, S. K., Roellig, T. L., Lodders, K., & Freedman, R. S. 2006, *ApJ*, 647, 552
- Saumon, D., et al. 2007, *ApJ*, 656, 1136
- Schmidt, S. J., West, A. A., Burgasser, A. J., Bochanski, J. J., & Hawley, S. L. 2010, ArXiv e-prints
- Scholz, R. 2010, ArXiv e-prints
- Skrutskie, M. F., et al. 2006, *AJ*, 131, 1163
- Smart, R. L., et al. 2009, ArXiv e-prints

- Stephens, D. C., Leggett, S. K., Cushing, M. C., Marley, M. S., Saumon, D., Geballe, T. R., Golimowski, D. A., Fan, X., & Noll, K. S. 2009, *ApJ*, 702, 154
- Tinney, C. G., Burgasser, A. J., Kirkpatrick, J. D., & McElwain, M. W. 2005, *AJ*, 130, 2326
- Vacca, W. D., Cushing, M. C., & Rayner, J. T. 2003, *PASP*, 115, 389
- Vrba, F. J., et al. 2004, *AJ*, 127, 2948
- Warren, S. J., et al. 2007, *MNRAS*, 381, 1400
- York, D. G., et al. 2000, *AJ*, 120, 1579